

A sequence of elastic patterns in a sheared bent sheet

D. Gimeno,^{1,*} B. K. Meghwar,¹ G. Fisher,¹ R. S. Hutton,¹ E. Hamm,^{2,†} and J. A. Hanna^{1,‡}

¹*Department of Mechanical Engineering, University of Nevada,
1664 N. Virginia St. (0312), Reno, NV 89557-0312, U.S.A.*

²*Departamento de Física, Facultad de Ciencia,
Universidad de Santiago de Chile, Av. Víctor Jara 3493,
Estación Central, Santiago 9160000, Chile*

(Dated: February 18, 2026)

We document a sequence of bifurcations and elastic patterns in sheared bent sheets of intermediate aspect ratio. The sheets undergo inversion of curvature through the passage of localized features, often in S-shaped pairs. Nested force-displacement hysteresis loops provide experimental evidence for snaking. Several mechanisms for coarsening and refinement of the patterns are observed, including splitting, merging, and escape through open boundaries. While most forces, including that required for full snap-through, scale with the length of the sheet, the initial drop in force upon pattern nucleation decreases rapidly with length.

Keywords: Thin structures, snap through, localization, snaking

I. INTRODUCTION

Thin elastic plates and shells under loading or confinement are a pattern-forming system with a history of influence on developments in bifurcation theory and nonlinear dynamics, such as the interrelated study of cellular buckling and homoclinic snaking [1]. A few interesting examples of work at the junction of these fields may be found in [1–9] and in other references discussed in the reviews [10, 11]. Conformational changes in such two-dimensional thin structures are characterized by inhomogeneous and often highly localized elastic deformations [12–15]. Such phenomena may be observed in many settings, including aircraft panels, which often operate in a dynamic post-buckled regime [16].

In this paper, we report experimental observations of a sequence of bifurcations and patterns previously informally presented in [17]. The context is one in which a plate or shell structure is inverting the orientation of its curvature; rather than homogeneous snap-through, this process occurs by the passage of localized zones which form the units of the observed patterns [18–26]. We here refer to such zones as “crumples”. We explore the sequence of patterns and bifurcations through force-displacement hysteresis loops of various sizes for sheets in a range of intermediate aspect ratios. These reveal a structure of solution branches consistent with snaking, a phenomenon in which different numbers of unit cells of a pattern can exist in overlapping ranges of parameters (see [27, 28] for reviews). We also briefly examine the forces and drops in force associated with these processes.

While the patterns we discuss resemble those well known in plate and shell buckling settings such as the pressurization and/or axial compression and/or torque of cylinders or spheres, not only the shear-like and partially open boundary conditions we employ, but the *evolution* of the patterns, are of a different type than those previously studied. Rather than sequential nucleation of cells on a static grid [4–8, 29–34], we observe refining and coarsening (up to complete elimination) of the pattern through events such as splitting or merging, entrance or escape, enabled by mobility of its fully elastic constituent crumples. Some refinement and coarsening were also documented in the

* D.Gimeno@sussex.ac.uk

† luis.hamm@usach.cl

‡ jhanna@unr.edu

early systematic experiments of Yamaki [35], but without details of the mechanism; entrance or escape were precluded by closed boundary conditions. An example of some type of merging can be found in Ravulapalli [36]. Evensen [37] notes that “the buckling pattern shifted and moved as it developed”. The observations reported here are both qualitatively different and more extensive.

II. METHODS

Measurements were taken of thin polyester sheets (0.003 ± 0.0002 inch thick shim stock, Artus Corp., Englewood, NJ, USA), with lengths in the range of 5-12 inch, mounted in a quarter-cylinder configuration with 4 inch free span (2.55 inch radius), their flat sides attached to parallel beams. One beam was fixed and rigid, and the other was a flexible cantilever attached to a mobile translation stage (Thorlabs, Inc., Newton, NJ, USA). Some observations were also made of longer sheets. As the material is mildly anisotropic, sheets were oriented with their machine direction parallel to the beams. Sheets were attached to the beams using rubber adhesive polypropylene cloth mounting tape, then secured with an additional clamping plate and corner clamps to prevent edge peeling. Alignment was achieved with additional positioning stages, and movement of the cantilever boundary was guided by four stabilizers to prevent twisting or deflection. Still, errors on the order of half a percent (1-2 mm relative to a sheet dimension of 150-300 mm) are expected, larger than an estimated error of 0.5 mm in free span width and length. The samples were quasistatically sheared by laterally displacing the cantilever boundary. The sheets transition, through a sequence of bifurcations and stable patterns, from an initial unimodal configuration (hereafter the “U” state), to a final multimodal configuration (“M” state). The experimental arrangement is shown in Figure 1, with U and M states for a 12 inch long sheet.

The cantilever was machined from a 24 inch long, 1 inch thick aluminum plate, leaving two thin beams approximately 5.31 inch long and 0.05 inch thick. A mild iron target was attached to one beam to enable measurement of deflection using an inductive sensor (Baumer Ltd., Southington, CT, USA), attached to a soldered external piece bolted to the cantilever. The stage-cantilever-sensor arrangement was calibrated by pushing against a rigid object, and by pushing against a load cell (Sentran LLC, Ontario, CA, USA). This allowed us to relate the position of the stage, the deflection of the cantilever, and the force applied by the cantilever. Displacements reported are those of the sheet edge mounted on the deflected end of the cantilever, not the base of the cantilever mounted on the stage. The cantilever is operated in a linear force-deflection regime. From the deadload measurements, we also determined that the stage backlash can be empirically corrected throughout the relevant load regime by applying a 5 micron shift between forward and backward load curves. This is consistent with manufacturer-supplied accuracy and backlash values. Force data from the sensor had a noisy width of 0.008 Newton, and was smoothed using a Gaussian filter (Matlab smoothdata function which has an SD of 1/5 of window, window 50, acquired at 100 Hz) for the purpose of clearer visualization. An example of the qualitative effects of this smoothing is shown in Figure 2. The effects can also be inferred from the slope artifacts seen on the force-displacement curves, although we note that slightly sloped jumps occur in a system loaded by a compliant structure such as a cantilever (not strictly displacement controlled). A few small and short-lived events occurring in longer sheets are masked by the rates and filtering used here. Sensor drift of the same order as the noise was occasionally observed over periods spanning tens of minutes.

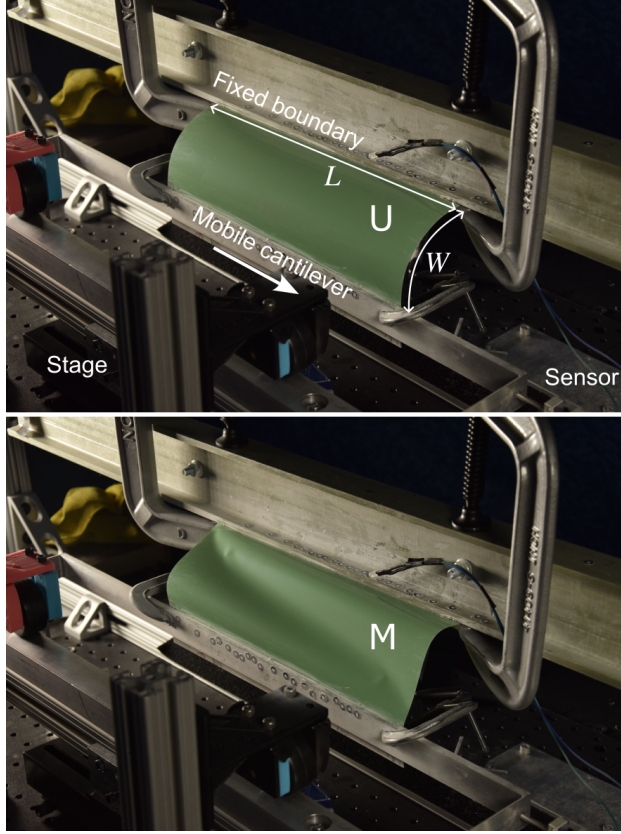


FIG. 1. Experimental setup showing a laterally translating, instrumented boundary, and a 12 inch long (L), 4 inch wide (W), 0.003 inch thick sheet of polyester. Top: sheet is bent into a quarter-circle in the unsheared unimodal U state. Bottom: the lower boundary has moved rightward parallel to the fixed boundary, shearing the sheet into the multimodal M state, in which two small puckers are also visible.

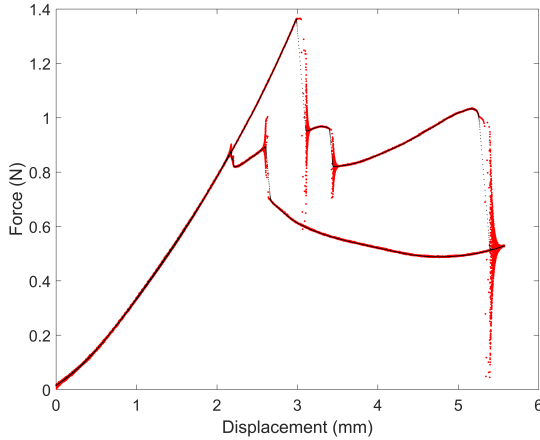


FIG. 2. Unfiltered (red) and filtered (black) force-displacement loops, traversed clockwise. The black curve is the same as that in Figure 6 in Section IV below.

The stage is moved at a speed of 0.01 mm/s, with accelerations of 1 mm/s² at the beginning and end of the loops. Executing a single full loop takes about 12-18 minutes. We zero the sensor (corresponding to the calibration zero) on the cantilever without any sample attached, then attach

and clamp a sheet and move the stage until the sensor is zeroed again. This serves as a reference symmetric unsheared “U” state of the sheet, corresponding to the zero of our displacement. As can be gleaned from the figures, this zeroing was only performed approximately; errors may be as much as 120 microns. The stage is moved until the sheet reaches some M configuration. The displacement to effect this and other transitions becomes smaller with increasing aspect ratio of the sheet, as it is bounded by the straightening of the long diagonal [38]. The stage is programmed to go back and forth between reference U and M positions and various points of interest in loops of different lengths, to explore different branches of equilibria. Data is acquired after “warming up” the system by cycling it around the largest loop four or five times at a speed of the same order of magnitude as that used for data collection.

Crumples are filmed with a Nikon D5300 camera, with the sheets illuminated from the side. Crumple positions from Video 2 (24 Hz, 8x original speed) were tracked using several Matlab [39] functions by a code modified from that generated by Gemini [40] (in response to prompts such as “keep track of blobs”, “I want to see visualization”), then verified and further modified using overlay comparison with video. Images are converted to grayscale, separated into upper and lower regions with a hand-drawn diagonal line, and half of the image is grayscale-inverted, before both halves are binarized using dynamic thresholds. Blobs are detected as 4-connected regions and infilled to be simply connected, with regions discarded according to size and aspect ratio thresholds, along with noisy artifacts within 10px of the sheet boundaries. A few additional spurious regions are identified by comparison with video and manually discarded. The top (bottom) points of the boundaries for upper (lower) blobs serve as imperfect proxies for crumple core positions. This data is not filtered.

III. PRELIMINARY OBSERVATIONS

Let us first introduce the phenomena of interest through observations. An organized sequence of dynamics can be seen in Videos 1-2, in which long (high aspect ratio) bent sheets are subject to lateral boundary displacement, resulting in a sequence of quasi-1D patterns of crumples. Note that the deformation shown in V1 is due to boundary displacement in the opposite direction as in V2 and all the experiments in this paper; it is effectively a mirror image of the behavior. The sheet is also about twice as large and thick, with longer aspect ratio, and the boundary is moved more than two orders of magnitude faster, than in the experiments. Video 2 involves the same conditions as our highest aspect ratio experiments, detailed above in Section II.



Video 1. Patterns in 0.005 inch polyester shim stock, 48 inches long, bent into a quarter-circle with 10 inches free span, clamped with lower boundary moving laterally to the left and then to the right. The boundary is moved more than two orders of magnitude faster than in experiments used for data. Excerpt from [17].



Video 2. Patterns in 0.003 inch polyester shim stock, 12 inches long, bent into a quarter-circle with 4 inches free span, clamped with lower boundary moving laterally to the right and then to the left. The boundary is moved at 0.003 mm/s and the video is at 8x speed, at 24 Hz. Used for Figure 3. (Credit: C. Redman)

The transition from U to M and back in long sheets is as follows. First, a regular zipper of O-shaped oval indentations forms in rapid sequence in the U state. The crumples of this “crystal” then spread and subtly re-pair into a similar but more “fluid” array of S-shaped features, which move together as tightly bound pairs. Throughout this paper, we will refer to the O- and S-shaped pairs as “O-valleys” and “S-ridges”, reflecting two different types of connection between the crumples. Through a sequence of mergers and edge escapes, the S pattern coarsens until a single S remains, which is finally expelled through an edge. In this M state, small “puckers” can be seen, indicative of the instability of ridges (here valleys) to indentation [41]. These are potential nucleation sites for crumples, although this process has been shown to be complex, involving rapid transients in which small unstable crumples enter from inflection points in intermediate aspect ratio sheets [26]. Upon reversal of the boundary motion (the video breaks and re-starts after some of this motion), a single S-ridge is nucleated, and then its two constituent crumples separate with a hint of repulsion (explored in another paper [42]), before a new O-valley is nucleated in between, leading to strong repulsion and splitting of the single S-ridge into two S-ridges. This sequence of splitting continues, regularly or irregularly, until a full array of S-ridges returns, then subtly re-pairs into an array of O-valleys and contracts, before the valleys close, annihilating all the crumples and returning the system to the U state.

A detailed annotation of the sequence of events corresponding to Video 2 is shown in Figure 3 below. Several events of interest are labeled, and some states indicated on the right. Many pairwise motions of crumples, and overall rotation of the pairs due to forward and backward shear, can be seen. On top of this rotation can be seen the repulsion of the S before the first splitting event, during the return at around 110-115 seconds. After the second splitting, an “extra” crumple has been nucleated near the right edge (hence “4.5S”). The next event creates three crumples, while one S shifts rapidly rightward as indicated by the arrows; the resulting state has stray single crumples to the left and right of a 5S array (hence not “6S”), which pattern transitions to 6O. A similar S-pattern occurs early in the process when $5O + 1O = 6O$ transitions from O to S, before the two strays escape to give 5S. Also apparent are the rapid spreading (truncated by a pair nucleation event) and contraction respectively preceding and succeeding the subtle collective transitions from O to S and S to O. Different sequences of splittings, mergers, and escapes are observed in other sheets.

In Section IV, we further explore this and similar full loops of states, and internal loops within them, using a series of sheets of increasing aspect ratio, allowing for single or multiple cells (crumple pairs) of the pattern.

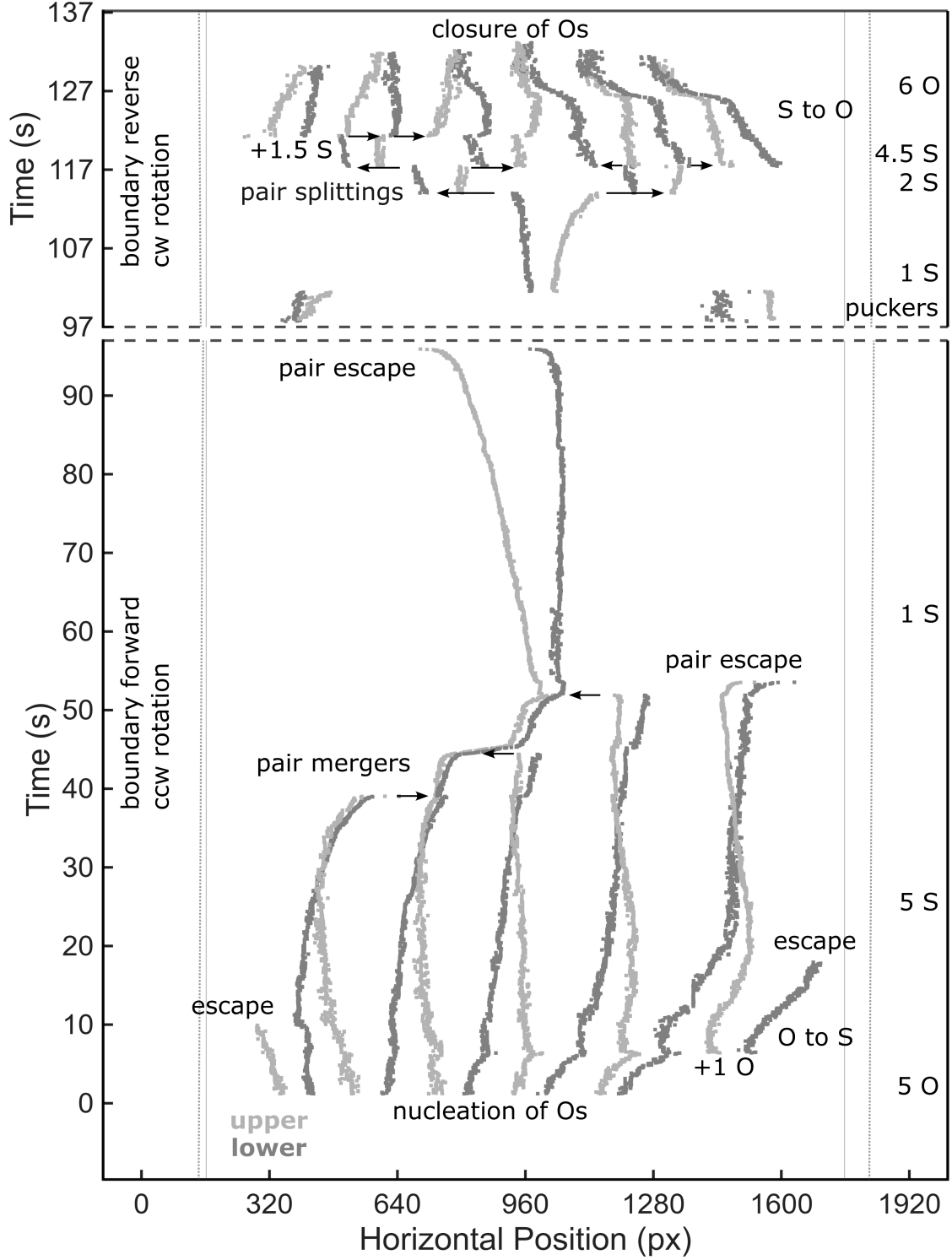


FIG. 3. Spacetime plot corresponding to Video 2. Horizontal locations of upper (grey) and lower (dark grey) crumples are given in pixels, with a correspondence of approximately 135-138 px/in on the secant plane, with values decreasing upwards in the sheet, and unknown error due to projection of the elevated center of the sheet. Grey lines indicate the spacetime locations of the fixed (solid) and moving (dotted, note slight slopes and jumps at the break) corners of the sheet. Some fast motions are indicated with arrows. Pair positions like the configuration at around 105 seconds correspond to a vertically oriented S-ridge. Details in text.

IV. RESULTS

In this section and in Appendix A we present force-displacement loops of various sizes for several sheets of intermediate aspect ratio, between 1.25 and 3. All loops shown are traversed clockwise, that is, the upper branch is followed to the right and the lower to the left. Reproducibility can be gleaned from the plots. Nearly all features of the loops are highly reproducible for individual sheets. The system is very sensitive to boundary conditions associated with alignment and particularly with clamping, leading to differences between sheets. While these experiments are an extension of the work begun in [26], we note that displacement rates here are significantly lower than the supposedly “quasistatic” rates used in that previous work. The sheets are also thinner and smaller, resulting in less violent release of elastic energy. These differences lead to the stable observation here of a few states only seen transiently in [26].

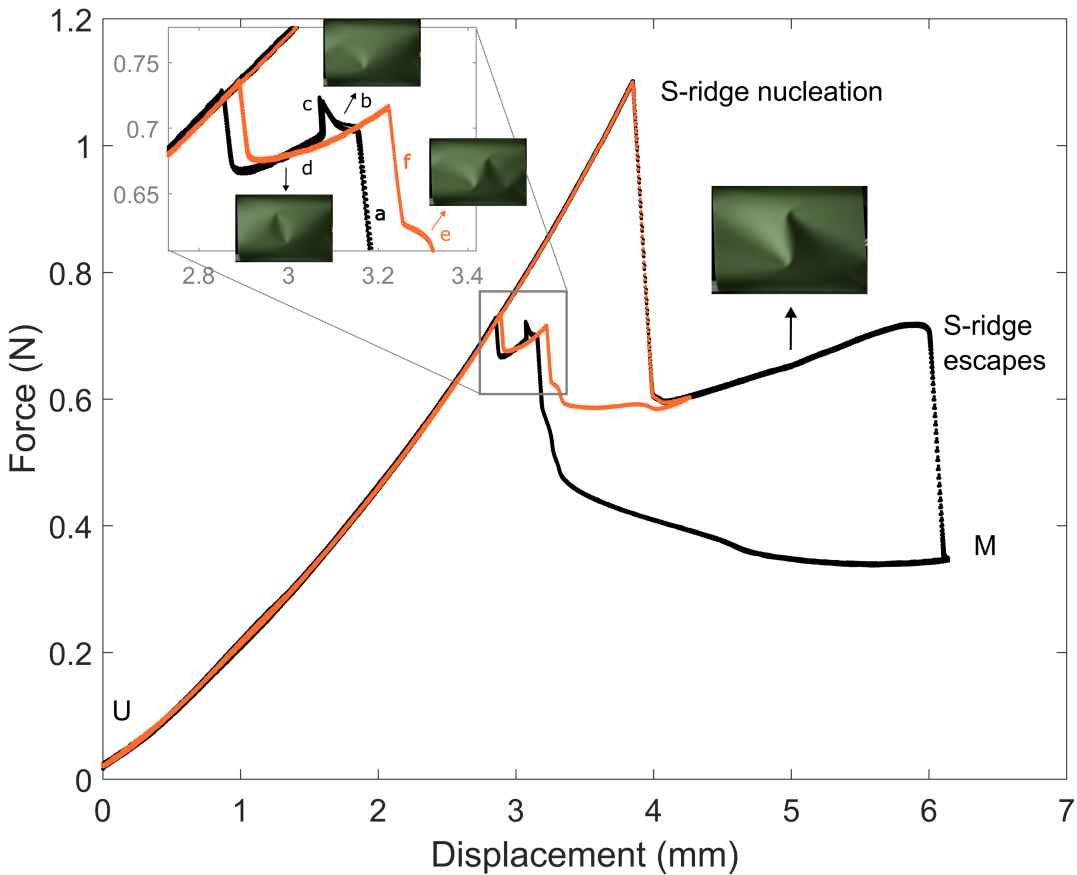


FIG. 4. Force-displacement loops, traversed clockwise, for a 5 inch long sheet: five full loops in black and two partial loops in orange. Some intermediate stable states are shown in the insets. Details in text.

Force-displacement loops for a 5 inch long sheet ($L/W = 1.25$) are shown in Figure 4, along with insets showing several intermediate stable states of interest. This sheet is long enough to admit about one unit cell of the pattern, consisting of two crumples in either an O or S configuration. The five black curves, which sit very closely on top of each other, correspond to a full loop between U and M states. The force increases monotonically with displacement until a large drop corresponding to the first bifurcation from the U state, resulting in a single S-ridge. The force increases monotonically

again until the final bifurcation expelling the S-ridge from the edge of the sheet, resulting in complete snap-through to the M state. Reversing the boundary shear and returning along the lower branch, there is a jump in force (a) to a short-lived single-crumple state (b), soon followed by a drop in force (c) corresponding to the edge-entrance of another crumple, which binds to the first to form an O-valley (d). The O-valley shrinks until it collapses with a final jump in force, bringing the sheet back onto the original U state branch. The two orange curves, also in very close agreement, correspond to a partial loop between U and a point shortly after the first bifurcation to an S-ridge. Upon return, the S-pair slowly rotates clockwise, until a new crumple enters from the lower right (e). During the jump (f), the upper crumple in the S-pair re-pairs with the newly entered crumple to form an O-pair, and then the lower crumple in the S-pair is expelled from the left edge, resulting in a single O-valley, whose closure returns the system to the original branch. This last intermediate process on the inner loop (orange) does not overlap with the corresponding part of the full loop (black), as the O-valleys in these cases are not identically shaped or situated.

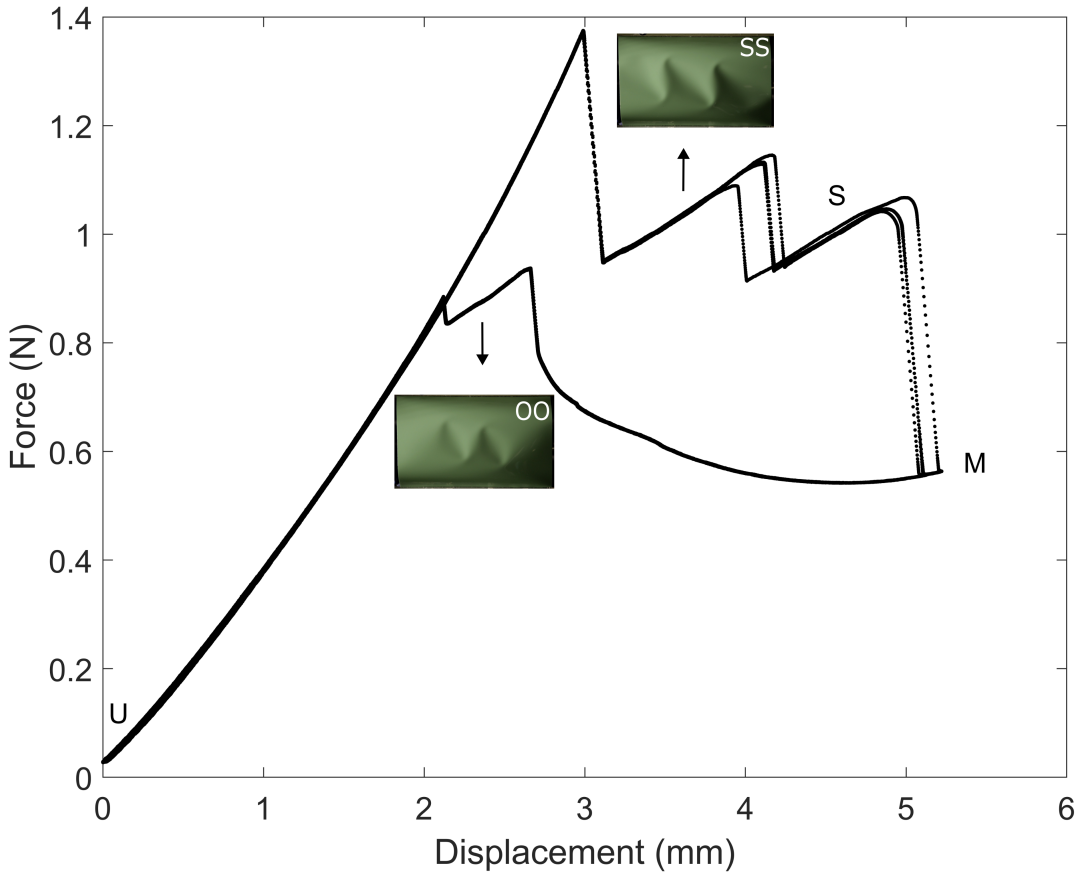


FIG. 5. Four force-displacement loops, traversed clockwise, for a 6 inch long sheet: increasing shear in red and decreasing shear in blue. Insets show stable states with two pairs of crumples in S-ridge and O-valley arrangements. Details in text.

Four full force-displacement loops for a 6 inch long sheet ($L/W = 1.5$) are shown in Figure 5, along with two insets. This small increase in sheet length provides enough room for an additional cell of the pattern. The first bifurcation and force drop results in a pair of S-ridges. These rotate until the next drop when one ridge is expelled from the edge. The remaining ridge rotates until it is expelled in the final bifurcation. On the return branch, a pair of O-valleys forms. These close

essentially simultaneously. Most features of the loops are highly reproducible, but the displacement at which S-ridges are expelled can vary.

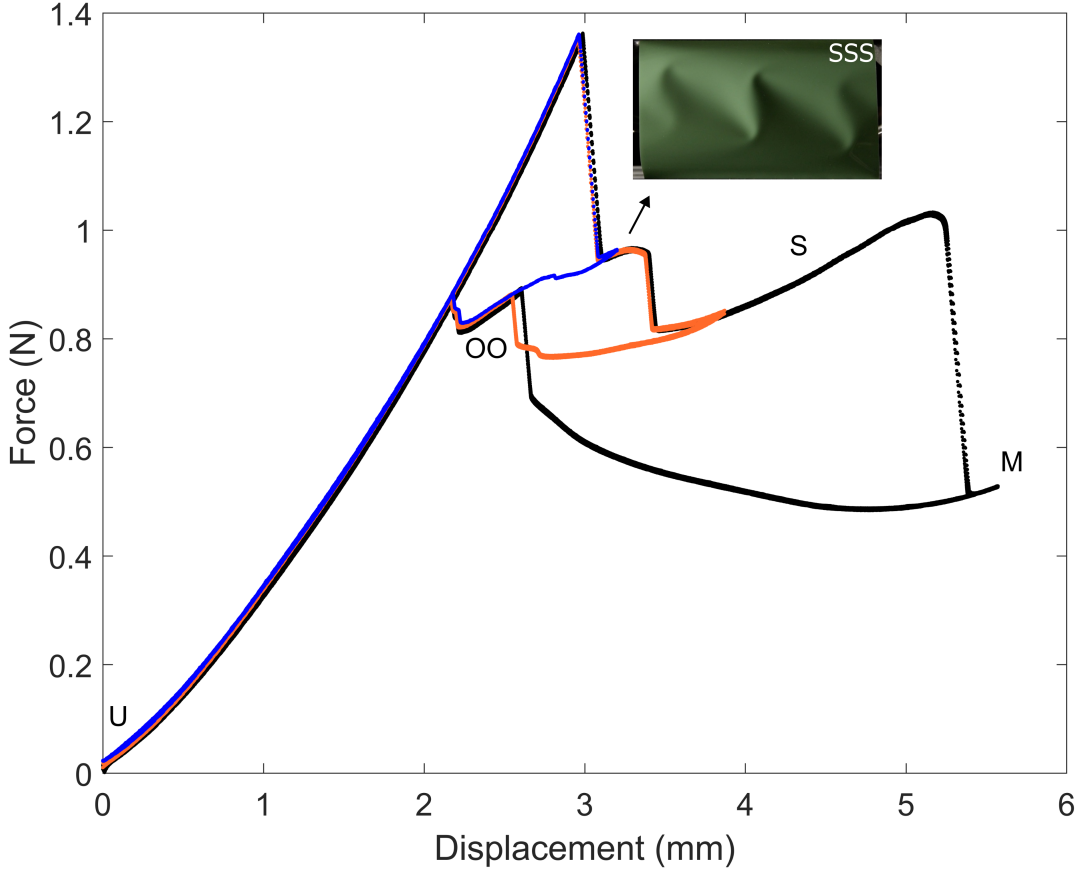


FIG. 6. Force-displacement loops, traversed clockwise, for a different 6 inch long sheet: four full loops in black and two partial loops each in orange and blue. Here the first stable state observed has three S-ridge pairs, as shown in the inset. Details in text.

Force-displacement loops for a different sheet of the same size are shown in Figure 6, along with an inset. Here a triple-S pattern forms instead of a double-S pattern, and exists over a shorter interval. This is an example of how sensitive this type of system is to boundary conditions. Here the four black curves are full loops, while the two each of orange and blue curves are partial loops between U and the intermediate S and triple-S states, respectively. The orange S branch shows a bit of hysteresis, with return deviating from forward. The creation of OO occurs through a re-pairing after nucleation of a crumple on the lower right (small shoulder) and then another on the upper left (large jump). This process can be compared with the behavior corresponding to e-f in Figure 4, described previously. On the blue branch, the SSS to OO transition occurs through expulsion of crumples on the upper right and lower left.

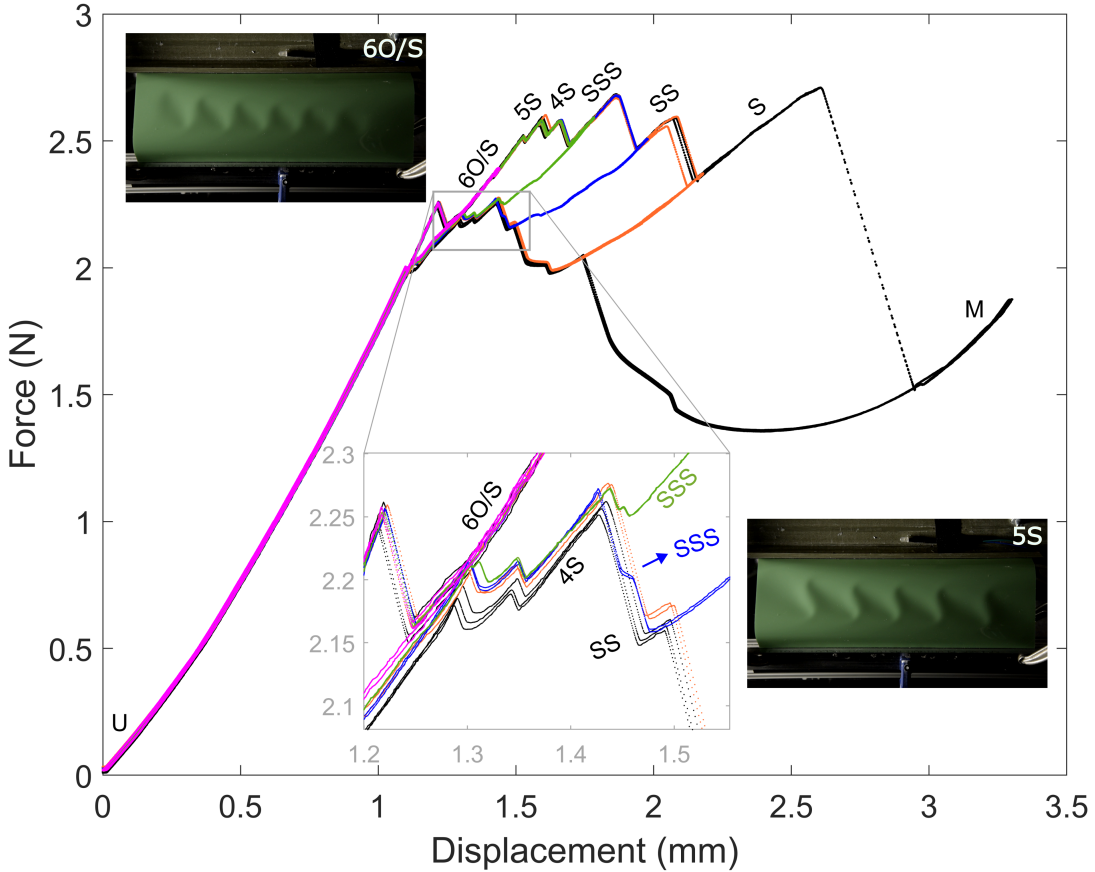


FIG. 7. Force-displacement loops, traversed clockwise, for an 11 inch long sheet: three full loops in black and two partial loops each in orange, blue, green, and pink. Details in text.

Force-displacement loops for an 11 inch sheet ($L/W = 2.75$) are shown in Figure 7. This longer sheet has room for more unit cells. Here the three black curves are full loops, while the two each of orange, blue, green, and pink curves are partial loops between U and several other states. The curves are complex but reproducible, with signatures of many small events. The transition from O to S pairing is too subtle to distinguish. Higher-number patterns are harder to access and interpret, likely because of released kinetic energy as well as interactions with the free edges, such as the induction of crumples. These effects also interfere with the ideal doubling sequence. However, it is clear that while going both forward and backward, the system visits identifiable branches containing one, two, three, four, and possibly more pairs of crumples that exist in overlapping regions of the boundary displacement. The least reproducible aspect of the curves is the transition from SS to S, which on this sheet proceeds through a merger rather than an escape. For this sheet, the coarsening sequence from 5S was: escape of rightmost S, escape of leftmost S, merging on the left, merging, escape.

Additional full and partial loop force-displacement data for various sheet lengths is included in Appendix A. While they do not directly correspond, the responses shown in Figure 7 and throughout the Appendix can be compared with the annotations of Video 2 in Figure 3. A portion of such curves corresponding to the breaking of an S-ridge just before splitting is measured more carefully in another paper [42].

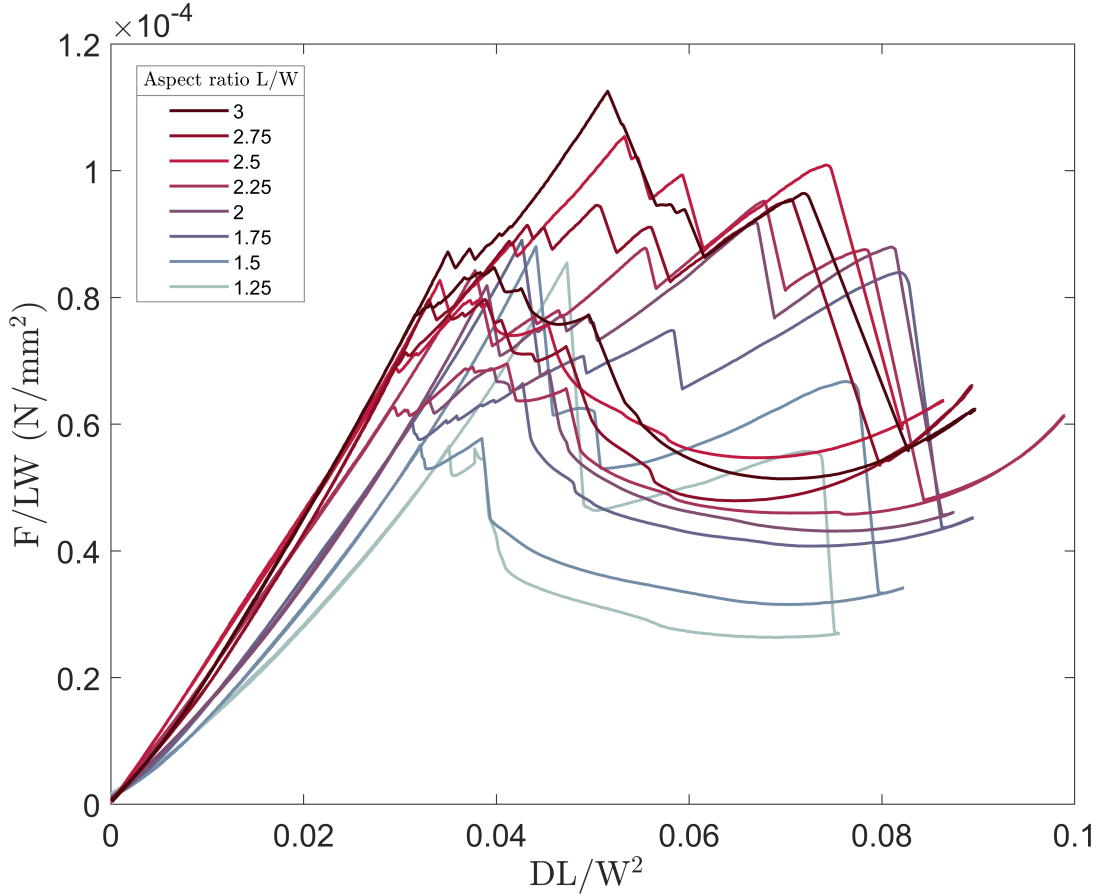


FIG. 8. Full force-displacement loops for sheets of lengths 5 to 12 inches (aspect ratios 1.25 to 3), with displacement D divided by the width W and multiplied by aspect ratio L/W , and force F divided by sheet area LW .

Figure 8 overlays full force-displacement loops for sheets. The displacement has been divided by the width W and then multiplied by aspect ratio L/W , because the normalized displacements at which bifurcations occur scale inversely with aspect ratio at large aspect ratios [26, 38]. The force has been divided by the total area of the sheet LW . Recall that W is not varied in these experiments. These simple scalings bring some aspects of the plots into rough correspondence, particularly for the longer sheets.

Basic information about forces is extracted from these loops and plotted on a log scale in Figure 9. This shows five relevant forces, divided by sheet area: the first (yield) peak and drop arising from the first bifurcation giving rise to the first O-valley(s), the last peak and drop from the escape of the last S-ridge to achieve final snap-through, and the maximum force, which for shorter sheets corresponds to an early peak and for longer sheets corresponds to later peaks, although these are not that different in value.

Several of the forces, in particular the last drop in force, approach flatness on this plot for longer sheets, meaning that they simply increase linearly with length (equivalent to area here, as we have not varied the width). The peak force might increase a bit faster, but this is not so meaningful as it corresponds to different features on the plots, at times coinciding with other forces shown. While the yield force over length (area) is roughly flat, the yield drop decreases rapidly with sheet length,

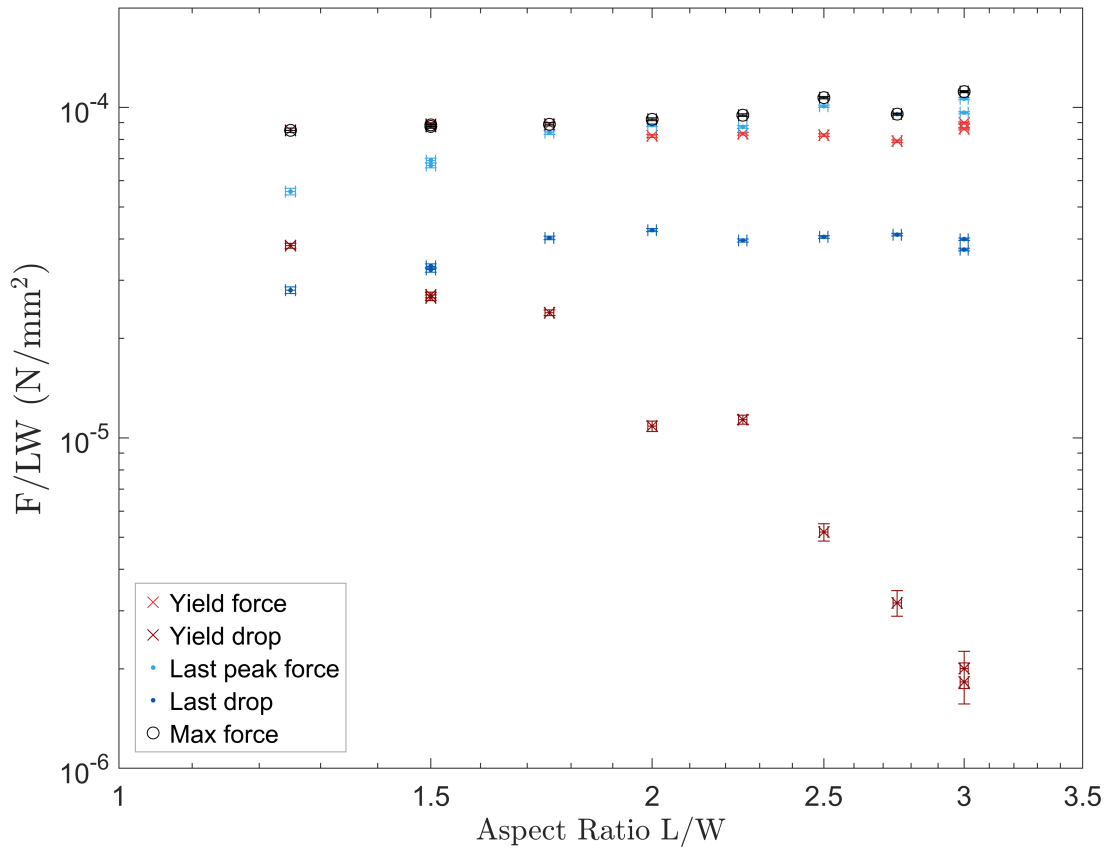


FIG. 9. Forces (divided by sheet area) corresponding to the loops used in Figure 8: the first (yield) force peak and corresponding drop in force, the last force peak and corresponding drop, and the maximum force, which is associated with different features among the curves, and at times coincides with other forces shown. Error bars denote uncertainty of individual measurements from noise and drift.

reflecting higher loads after restabilization for longer sheets, at least within this intermediate range of aspect ratios.

V. DISCUSSION

Our results provide experimental evidence for snaking in buckled plates. Figures such as 6 and 7 show multiple overlapping branches, each containing a different number of crumple pair unit cells. The utility of this concept in understanding buckled structures has been demonstrated in recent work employing finite element or PDE representations of shallow shells [4–8], and the present work suggests possible starting points for path following employing such methods. Our plots show similarities to those obtained by Yamaki [35, figures 3.47, 3.52b-e] and Eßlinger and Geier [32, figure 3.21]. One can also compare with the results of Ravulapalli [36, figures 9-14], who did not trace the response along internal return branches. These experiments were performed on cylindrical structures with quite different boundary conditions than the present work. It is also important to note that much experimental work on metallic or polymeric “cylindrical shells” was actually performed using bent sheets with a lap joint [29, 35] or butt strap joint [32], while some

used structures with a natural cylindrical state created by electrodeposition [30], spin-casting [31], or 3D-printing [36]. This distinction between bent plates and proper shells is often overlooked, and its consequences remain unclear.

Branches with five or more pairs, and O-pair regimes that exist in a small range of lower shears, are a bit more ambiguous to observe due to edge effects adding/subtracting individual crumple half-units, and are harder to access with internal loops in these sheets. There is additional complexity here because of the subtle transitions between O and S pairs, although we note interesting transitions were shown in very short cylinders in [32, figure 3.44b]. Furthermore, some of the subtle interactions between crumples can be attributed to the formation and breaking of “bonds” that form the subject of another paper [42]. The trends seen in these intermediate aspect ratio sheets were also informally observed at higher aspect ratios that allow for more unit cells. However, with these dimensions come greater sensitivity to boundary conditions, and smaller displacement ranges and jumps in force.

Our system has allowed us to observe several mechanisms for coarsening and refinement of the pattern. Of these the most interesting is the splitting of the S-ridge, which involves a bond breaking and weak repulsion between individual crumples (explored in [42]), then nucleation of an O-valley (related to the instability of ridges to indentation [41]) and concomitant strong repulsion between the resulting crumple S-ridge pairs. It is unknown whether such mechanisms are system-specific, or whether something analogous might be observed more generally across model pattern forming systems. Other mechanisms were enabled by the open boundaries of our system. Crumple induction events near boundaries might be compared with similar events in the interior [33, 43].

The classic O-valley pair, akin to the indentation obtained by poking a soda can, is often seen as the unit of static patterns on cylinders. While we observe these here in our open-boundary system, the highly mobile but tightly bound S-ridge pair appears to be the dominant motif enabling transitions between patterns and mediating the global snap-through of the structure.

Most forces in these sheets increase simply with sheet length or, equivalently here, area. For example, the final drops in force suggest that the energy of an isolated S-ridge in a long sheet is associated with a nearly-constant cross section away from the ridge. However, the initial yield drops show a rapid decline with length. Yield corresponds to the nucleation of O-valleys, which in longer sheets become shallower and play a more incremental role with respect to the full snap-through, which still requires a force that scales with length.

VI. CONCLUSIONS

A sequence of bifurcations and patterns in an elastic sheet bring part of a cylinder to a snapped-through configuration and back again, with an S-shaped pair motif playing an important role. Partial loops reveal behavior consistent with snaking. Mechanisms enabling these transitions, including splitting, merging, and escape of S-pairs, were discussed, along with some aspects of the forces required.

ACKNOWLEDGMENTS

We thank R. Groh for many helpful discussions before and during the writing of the paper, T. Yu for early discussions and ideas, B. Nagy for machining cantilevers, C. Redman for help with videos, and A. Robinson and J. Rudfelt for help with experiments. JAH acknowledges support from the U.S. National Science Foundation under grant CMMI-2210797. EH is grateful for the support of DICYT (USACH) under grant 042431HH.

ADDITIONAL FILES

Videos: <http://doi.org/10.5281/zenodo.18487904>

Data: <https://doi.org/10.5281/zenodo.18487934>

AUTHOR CONTRIBUTIONS

EH and JAH conceived and guided the study. DG and EH designed the apparatus. DG performed the experiments. GF and RSH contributed to the apparatus and performed early exploratory experiments. DG, BKM, EH, and JAH analyzed data and made figures. JAH wrote the first draft, and DG and EH contributed to the final draft.

[1] G. W. Hunt, G. J. Lord, and A. R. Champneys. Homoclinic and heteroclinic orbits underlying the post-buckling of axially-compressed cylindrical shells. *Computer Methods in Applied Mechanics and Engineering*, 170:239–251, 1999.

[2] J. Horák, G. J. Lord, and M. A. Peletier. Cylinder buckling: the mountain pass as an organizing center. *SIAM Journal on Applied Mathematics*, 66:1793–1824, 2006.

[3] J. M. T. Thompson and J. Sieber. Shock-sensitivity in shell-like structures: With simulations of spherical shell buckling. *International Journal of Bifurcation and Chaos*, 26(2):1630003, 2016.

[4] T. Kreilos and T. M. Schneider. Fully localized post-buckling states of cylindrical shells under axial compression. *Proceedings of the Royal Society A*, 473:20170177, 2017.

[5] R. M. J. Groh and A. Pirrera. On the role of localizations in buckling of axially compressed cylinders. *Proceedings of the Royal Society A*, 475:20190006, 2019.

[6] G. W. Hunt, R. M. J. Groh, and T. J. Dodwell. Maxwell tipping points: the hidden mechanics of an axially compressed cylindrical shell. *Proceedings of the Royal Society A*, 476:20200273, 2020.

[7] R. M. J. Groh, G. W. Hunt, and A. Pirrera. Snaking and laddering in axially compressed cylinders. *International Journal of Mechanical Sciences*, 196:106297, 2021.

[8] R. M. J. Groh and G. W. Hunt. Localization and snaking in axially compressed and internally pressurized thin cylindrical shells. *IMA Journal of Applied Mathematics*, 86:1010–1030, 2021.

[9] D. Ehrhardt, L. N. Virgin, and S. M. Spottswood. Experiments on probing the configuration space of post-buckled panels. *Journal of Applied Mechanics*, 87:121005, 2020.

[10] J. M. T. Thompson. Advances in shell buckling: Theory and experiments. *International Journal of Bifurcation and Chaos*, 25(1):1530001, 2015.

[11] A. R. Champneys, T. J. Dodwell, R. M. J. Groh, G. W. Hunt, R. M. Neville, A. Pirrera, A. H. Sakhaei, M. Schenk, and M. A. Wadee. Happy catastrophe: Recent progress in analysis and exploitation of elastic instability. *Frontiers in Applied Mathematics and Statistics*, 5:34, 2019.

[12] T. A. Witten. Stress focusing in elastic sheets. *Reviews of Modern Physics*, 79:643–675, 2007.

[13] M. Ben Amar and Y. Pomeau. Crumpled paper. *Proceedings of the Royal Society of London. Series A*, 453:729–755, 1997.

[14] S. Chaïeb, F. Melo, and J.-C. Géminard. Experimental study of developable cones. *Physical Review Letters*, 80:2354–2357, 1998.

[15] E. Cerda and L. Mahadevan. Conical surfaces and crescent singularities in crumpled sheets. *Physical Review Letters*, 80:2358–2361, 1998.

[16] S. M. Spottswood, B. P. Smarslok, R. A. Perez, T. J. Beberniss, B. J. Hagen, Z. B. Riley, K. R. Brouwer, and D. A. Ehrhardt. Supersonic aerothermoelastic experiments of aerospace structures. *AIAA Journal*, 59(12):5029–5048, 2021.

[17] R. S. Hutton, E. Vitral, J. A. Hanna, and E. Hamm. Crumple dynamics mediating snap-through. <https://www.youtube.com/watch?v=y02SppD0sXA>, 2022.

[18] L. Berke and R. L. Carlson. Experimental studies of the postbuckling behavior of complete spherical shells. *Experimental Mechanics*, 8:548–553, 1968.

- [19] S. Kyriakides. Propagating instabilities in structures. *Advances in Applied Mechanics*, 30:67–189, 1994.
- [20] J. M. F. G. Holst and C. R. Calladine. Inversion problems in elastic thin shells. *European Journal of Mechanics, A/Solids*, 13(4 suppl.):3–18, 1994.
- [21] L. Pauchard and S. Rica. Contact and compression of elastic spherical shells: the physics of a ‘ping-pong’ ball. *Philosophical Magazine B*, 78(2):225–233, 1998.
- [22] T. Mora and A. Boudaoud. Thin elastic plates: On the core of developable cones. *Europhysics Letters*, 59(1):41–47, 2002.
- [23] M. Das, A. Vaziri, A. Kudrolli, and L. Mahadevan. Curvature condensation and bifurcation in an elastic shell. *Physical Review Letters*, 98:014301, 2007.
- [24] B. Roman and A. Pocheau. Stress defocusing in anisotropic compaction of thin sheets. *Physical Review Letters*, 108:074301, 2012.
- [25] V. Deshpande, O. Myers, G. Fadel, and S. Li. Transient deformation and curvature evolution during the snap-through of a bistable laminate under asymmetric point load. *Composites Science and Technology*, 211:108871, 2021.
- [26] R. S. Hutton, E. Vitral, E. Hamm, and J. Hanna. Buckling mediated by mobile localized elastic excitations. *PNAS Nexus*, 3:pgae083, 2024.
- [27] E. Knobloch. Spatial localization in dissipative systems. *Annual Review of Condensed Matter Physics*, 6:325–359, 2015.
- [28] J. H. P. Dawes. The emergence of a coherent structure for coherent structures: localized states in nonlinear systems. *Philosophical Transactions of the Royal Society A*, 368:3519–3534, 2010.
- [29] L. A. Harris, H. S. Suer, and W. T. Skene. Model investigations of unstiffened and stiffened circular shells. *Experimental Mechanics*, 1:1–9, 1961.
- [30] B. O. Almroth, A. M. C. Holmes, and D. O. Brush. An experimental study of the buckling of cylinders under axial compression. *Experimental Mechanics*, 4:263–270, 1964.
- [31] R. C. Tennyson. Buckling modes of circular cylindrical shells under axial compression. *AIAA Journal*, 7(8):1481–1487, 1969.
- [32] M. Esslinger and B. Geier. *Postbuckling Behavior of Structures*. CISM No. 236. Springer - Verlag, Wien - New York, 1975.
- [33] J. Marthelot, P.-T. Brun, F. López Jiménez, and P. M. Reis. Reversible patterning of spherical shells through constrained buckling. *Physical Review Materials*, 1:025601, 2017.
- [34] Y. Timounay, R. De, J. L. Stelzel, Z. S. Schrecengost, M. M. Ripp, and J. D. Paulsen. Crumples as a generic stress-focusing instability in confined sheets. *Physical Review X*, 10:021008, 2020.
- [35] N. Yamaki. *Elastic Stability of Circular Cylindrical Shells*. North-Holland, Amsterdam, 1984.
- [36] V. Ravulapalli, G. Raju, and V. Narayananmurthy. Experimental studies on snaking in 3D-printed cylindrical shells under axial compression using photogrammetry. *Proceedings of the Royal Society A*, 480:20230631, 2024.
- [37] D. A. Evensen. High-speed photographic observation of the buckling of thin cylinders. *Experimental Mechanics*, 4:110–117, 1964.
- [38] T. Yu and J. A. Hanna. Bifurcations of buckled, clamped anisotropic rods and thin bands under lateral end translations. *Journal of the Mechanics and Physics of Solids*, 122:657–685, 2019.
- [39] The MathWorks Inc. MATLAB 2025a. <https://www.mathworks.com>.
- [40] Google. Gemini 3 Pro [Large Language Model]. <https://gemini.google.com>, 2025.
- [41] B. A. DiDonna. Scaling of the buckling transition of ridges in thin sheets. *Physical Review E*, 66:016601, 2002.
- [42] D. Gimeno, E. Hamm, and J. A. Hanna. Elastic crumple pair potentials. in preparation.
- [43] T. A. Witten and A. Movsheva. Sub-singularities for shaping thin sheets. *The European Physical Journal Special Topics*, <https://doi.org/10.1140/epjs/s11734-025-01903-6>, 2025.

Appendix A: Additional data

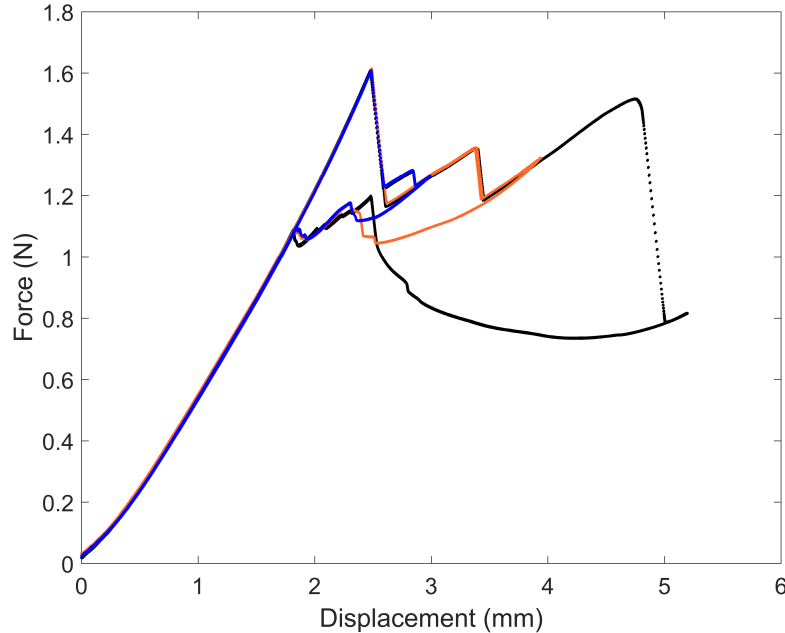


FIG. 10. Force-displacement loops, traversed clockwise, for a 7 inch long sheet ($L/W = 1.75$): three full loops in black and two partial loops each in orange and blue.

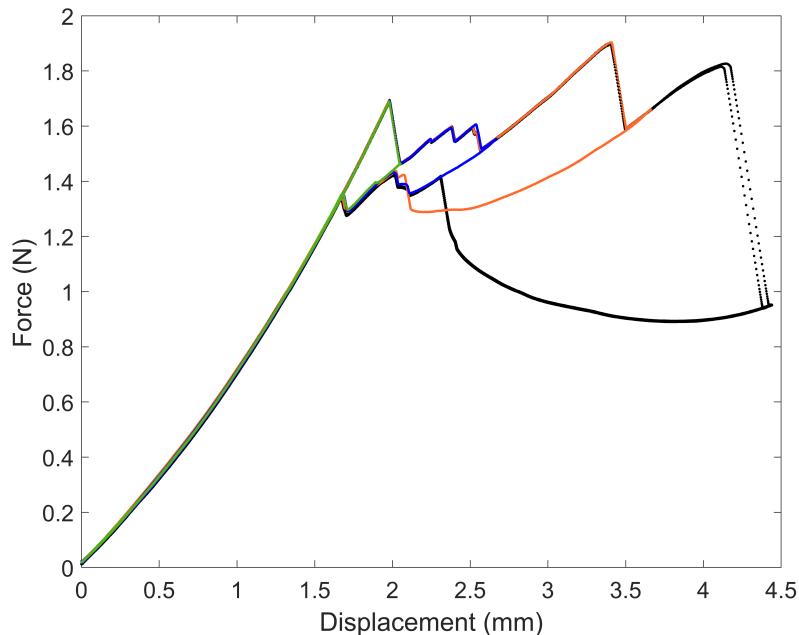


FIG. 11. Force-displacement loops, traversed clockwise, for an 8 inch long sheet ($L/W = 2$): two full loops in black and one partial loop each in orange, blue, and green.

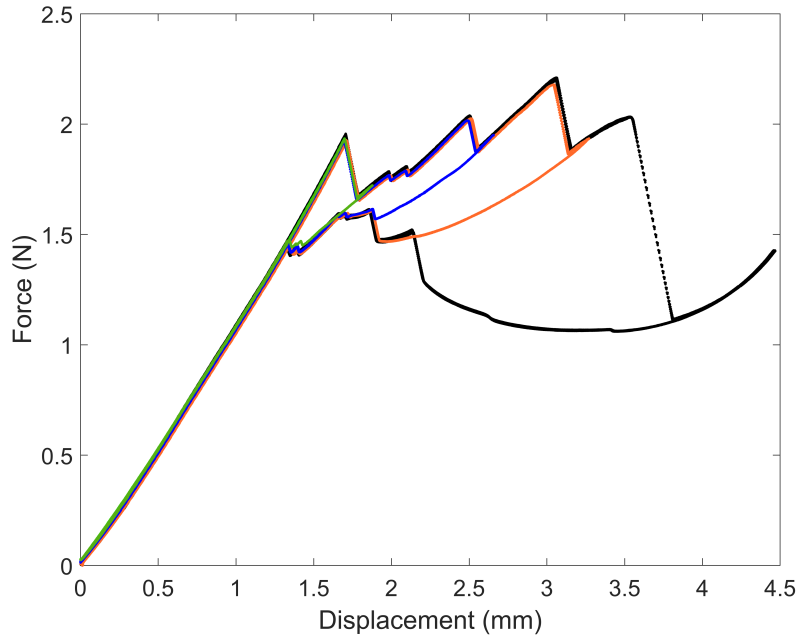


FIG. 12. Force-displacement loops, traversed clockwise, for a 9 inch long sheet ($L/W = 2.25$): four full loops in black and two partial loops each in orange, blue, and green.

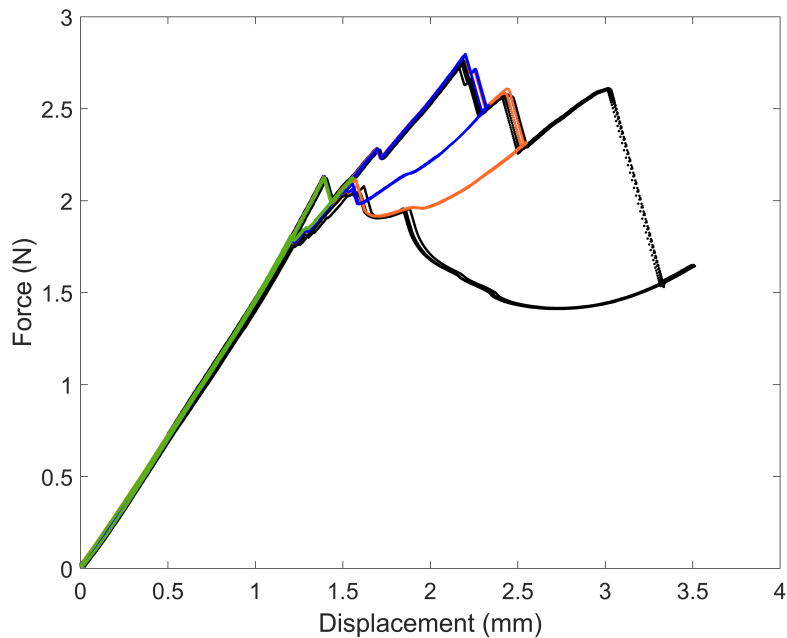


FIG. 13. Force-displacement loops, traversed clockwise, for a 10 inch long sheet ($L/W = 2.5$): five full loops in black and three partial loops each in orange, blue, and green.

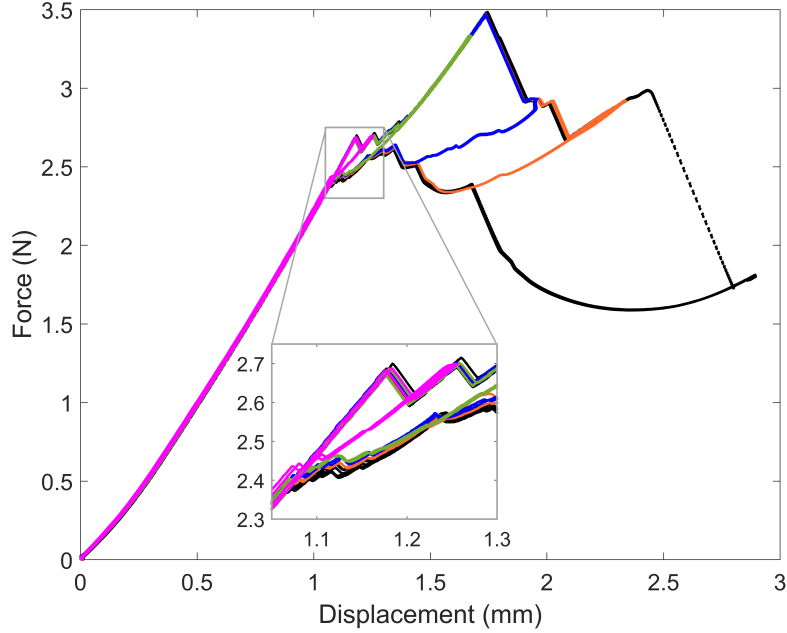


FIG. 14. Force-displacement loops, traversed clockwise, for a 12 inch long sheet ($L/W = 3$): five full loops in black and two partial loops each in orange, blue, green, and pink.

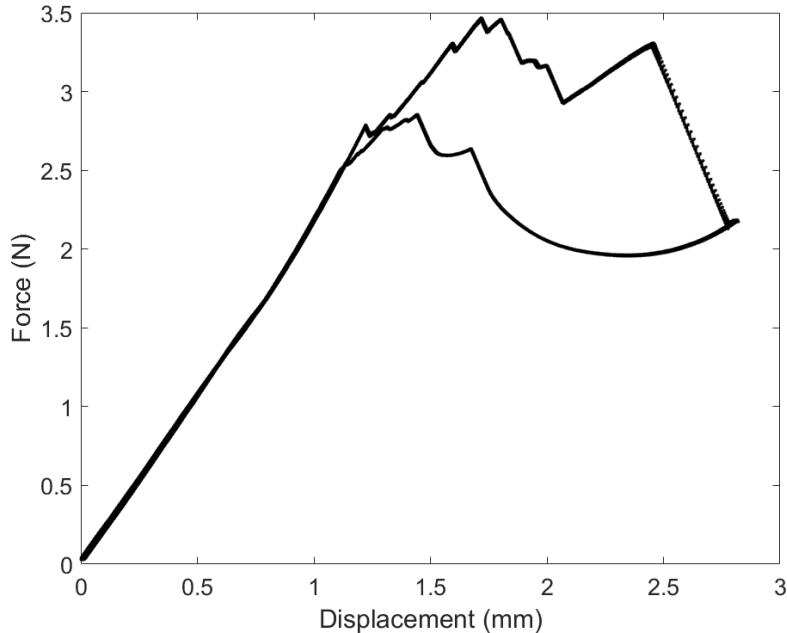


FIG. 15. Six force-displacement loops, traversed clockwise, for a different 12 inch long sheet than that of Figure 14. Note different behavior near the highest peak. For this sheet, the coarsening sequence from 5S was: escape of leftmost S, escape of rightmost S, merging on the left, merging, escape. On the return branch, the single S jumped directly to 4S. Note differences with the sequence for the different 12 inch sheet in Figure 3 and similarities with most of the coarsening sequence for the 11 inch sheet in Figure 7.